J. Electroanal. Chem., 138 (1982) 401–423
Elsevier Sequoia S.A., Lausanne – Printed in The Netherlands

DETERMINATION OF SPECIFIC ADSORPTION OF SOME SIMPLE ANIONS AT A POLYCRYSTALLINE SILVER–AQUEOUS INTERFACE USING DIFFERENTIAL CAPACITANCE AND KINETIC PROBE TECHNIQUES

D. LARKIN *, KENDALL L. GUYER, JOSEPH T. HUPP and MICHAEL J. WEAVER **

Department of Chemistry, Michigan State University, East Lansing, MI 48824 (U.S.A.)

(Received 8th September 1981; in revised form 12th March 1982)

ABSTRACT

The specific adsorption of chloride, bromide, iodide, azide, and thiocyanate has been studied at an electropolished polycrystalline silver–aqueous interface using differential capacitance measurements. For chloride, bromide, and azide, quantitative estimates of the surface concentration of specifically adsorbed anions were obtained from capacitance–potential data in mixed fluoride electrolytes having a constant ionic strength of 0.5. The dependence of the measured capacitance upon the ionic strength of sodium fluoride was also investigated in order to check the behavior of the polycrystalline surface in comparison with the predictions of conventional double-layer models. Estimates of the specifically adsorbed charge densities of chloride, bromide, and thiocyanate anions were also obtained from a "kinetic probe" technique, which entailed monitoring the response of the outer-sphere reduction rate of $Co(NH_3)_5F^{2+}$ and $Co(NH_3)_6^{3+}$ to the addition of the appropriate adsorbing anion. At the average potential of zero charge for the polycrystalline silver surface, the standard free energies of adsorption $-\Delta G_a^0$ for chloride, bromide, and azide were found to be within ca. 5 kJ mol^{-1} of the corresponding quantities obtained at mercury electrodes. However, significantly greater increases in $-\Delta G_a^0$ in the sequence $Cl^- < N_3^- < Br^-$ are seen at silver compared to mercury. Electrochemical roughening in chloride media, giving silver surfaces displaying intense surface Raman scattering, yields only minor changes in the surface concentration of specifically adsorbed chloride anions.

INTRODUCTION

Although the adsorption of a variety of ions and molecules have been studied at the mercury–aqueous interface, relatively little adsorption data have been gathered at solid metal surfaces. We have recently been examining the kinetics of mechanistically simple electrode reactions at a variety of solid metals as well as at mercury in order to identify the roles played by the metal surface in influencing the energetics of electron transfer [1–4]. In order to interpret the kinetic data in this manner, it is necessary to have information on the double-layer composition, including the extent

* Permanent address: Department of Chemistry, Towson State University, Towson, MD 21204, U.S.A.
** To whom correspondence should be addressed.

of specific ionic adsorption. In addition, studies of the adsorption thermodynamics of simple ligands, such as those that are involved as bridging ligands for heterogeneous electron transfer, should provide insight into the nature of the adsorbate–metal surface interactions.

Of the several solid metals under study in our laboratory, silver has been found to be particularly tractable. Its desirable features include the availability of a surface pretreatment procedure that enables surprisingly reproducible kinetic and adsorption data to be obtained [1], a wide polarizable potential range and the ability to induce extensive adsorption of a variety of anionic and neutral species as well as transition-metal reactants containing such ligands [4,5]. Silver electrodes are also the focus of considerable current attention as prototype systems for studies of surface-enhanced Raman spectroscopy (SERS) [6]. While SERS may yield valuable information on the molecular state of the adsorbate and the interactions with the metal surface, it does not allow an unambiguous determination of their surface concentration. Independent information on interfacial composition is therefore required in order to interpret the spectroscopic results fully, and in particular to ascertain the sensitivity of the SERS effect to the nature, as well as the surface concentration, of the Raman-active adsorbate. However, there have been surprisingly few studies of ionic adsorption at silver electrodes. The adsorption of chloride anions has been determined at various single crystal faces [7] and at a polycrystalline surface [8] by means of an analysis of capacitance data. Also, the adsorption of several anions at polycrystalline silver has been estimated using ellipsometry [9], and also a thin-layer voltammetric technique [10]. Although the study of single-crystal surfaces is preferable for understanding the fine details of double-layer structure, it is clearly important to examine the properties of polycrystalline electrodes in view of their practical utility.

We report here a study of the specific adsorption of several anions, including chloride, bromide, iodide, azide, and thiocyanate, at the polycrystalline silver–aqueous interface in order to compare the coordinating ability of silver for these simple bridging ligands with that of mercury electrodes. An additional reason for selecting azide and thiocyanate was that SERS for these adsorbates have recently been reported at silver [11].

The extent of specific adsorption has been obtained primarily from an analysis of differential capacitance data gathered for constant ionic strength mixtures having the general composition $(0.5 - c_b)\,M$ NaF $+ c_b\,M$ NaX, where c_b is the bulk concentration of the adsorbing anion X. Estimates of the specifically adsorbed charge density of X, q'_x, were also obtained from the response of the outer-sphere reduction rates of $Co(NH_3)_5F^{2+}$ and $Co(NH_3)_6^{3+}$ to the addition of the adsorbing anions. This "kinetic probe" technique can provide a sensitive supplemental method for detecting ionic adsorption when q'_x is small. In addition, differential capacitance data were obtained for sodium fluoride electrolytes over a range of ionic strengths and ac frequencies. This enables the behavior of our electrodes to be compared with the predictions of the modified double-layer models for polycrystalline electrodes that have been reviewed recently by Damaskin et al. [12].

EXPERIMENTAL

Materials and electrochemical cells

All solutions were prepared and all recrystallizations performed using water which was first distilled from alkaline permanganate and then subsequently distilled from a quartz non-boiling still (Model PB2, Dida-Sciences Inc., Montreal). Analytical reagents were generally used. Sodium fluoride was calcined in platinum crucibles at 750°C for 12 h before use in order to oxidize any organic impurities. Most other salts were twice recrystallized from water before use. Differential capacitance curves measured at a hanging mercury drop electrode in solutions prepared from these reagents were stable for at least several hours and conformed to literature values.

The electrochemical cell was of all-glass construction and consisted of two compartments separated by a fine glass frit. One compartment contained the counter and working electrodes, and the other the reference electrode. The counter electrode was a platinum spiral which was concentric with the working electrode and had a capacitance that was at least 100-fold larger. The polycrystalline silver working electrode was of rotating disk construction, consisting of a silver rod (99.999% assay, geometrical surface area 0.0491 cm^2) sheathed in Teflon and connected to a steel shaft. A commercial saturated calomel electrode (SCE) filled with saturated NaCl rather than KCl was used as the reference electrode, although all potentials are quoted versus the conventional (KCl) SCE. All solutions were deoxygenated using nitrogen, which could be bubbled through or passed over the cell solution. Residual traces of oxygen were removed either by passing the nitrogen through a column packed with BASF R3-11 catalyst heated to 140°C or through an acidified vanadous solution in contact with amalgamated zinc. The nitrogen was subsequently passed through several water presaturation columns before entering the cell. All glassware was soaked in 1:1 nitric/sulfuric acid mixtures for 24 h, then in water for at least one day and subsequently dried in an oven at 150°C before use.

Differential capacitance and cyclic voltammetric measurements

Cyclic voltammograms were obtained using a PAR Model 174A Polarographic Analyzer (EG & G Princeton Applied Research) and a Houston Model 2000 XY recorder. Differential capacitance measurements in the range 400–1500 Hz were obtained using a Wein configuration ac bridge of in-house design with a peak-to-peak amplitude of 10 mV. At lower frequencies (1–100 Hz) a phase-sensitive detection method was used. This employed a PAR Model 174 A Polarographic Analyzer, a Model PAR 170/50 Polarographic Analyzer a.c. interface, a PAR Model 5204 Lock-In Amplifier having an internal oscillator with a peak-to-peak amplitude of 10 mV and a Houston 2000 XY recorder. Under the conditions that the measured resistive component $R_m \lesssim 0.1/\omega C_m$, where ω is the angular frequency and C_m is the measured differential capacitance, then the quadrature component of the current is directly proportional to the differential capacitance and hence C_m can be recorded directly.

Electrode pretreatment

Silver electrodes were initially pretreated by following a procedure similar to that described by Valette and Hamelin [13]. The electrode was polished either on roughened glass or with 0.3 μm alumina on a polishing wheel (Buehler 44-1502-160) using water as a lubricant in both cases, immersed in an "electropolishing" solution (41 g l^{-1} NaCN, 44 g l^{-1} $AgNO_3$, 38 g l^{-1} K_2CO_3), and held at +0.20 V vs. SCE for 2 min. It was then removed, rinsed and transferred to a 0.1 *M* NaF solution while potentiostated at −0.7 V, and then held at −1.7 V for two 1 min periods with deaeration between cycles [1,2].

Figure 1(a) shows a typical cyclic voltammogram obtained at silver electrodes pretreated in this manner. The voltammogram is seen to contain a number of peaks which are unlikely to be due solely to double-layer charging. This structure was not diminished by continuous cycling nor by extensive polarization at very negative potentials (−1.7 V). Such behavior is consistent with the presence of adsorbed electroactive contaminants; these probably include some silver cyanide complexes, though we have no direct evidence of this. In order to remove such material from the electrode surface, the electrode pretreatment described above was modified by soaking the electrode in 2 *M* $HClO_4$ for 20 min, immediately following the electropolishing step. Figure 1(b) shows a typical cyclic voltammogram obtained at silver electrode using this modified pretreatment. The voltammogram is essentially featureless as would be expected if the current flow is chiefly due to double-layer charging. Electrodes pretreated in this way were found to have a roughness factor (rf) of about 1.1–1.3, determined by measuring the total charge required to strip a monolayer of underpotential deposited (upd) lead from the silver surface [14].

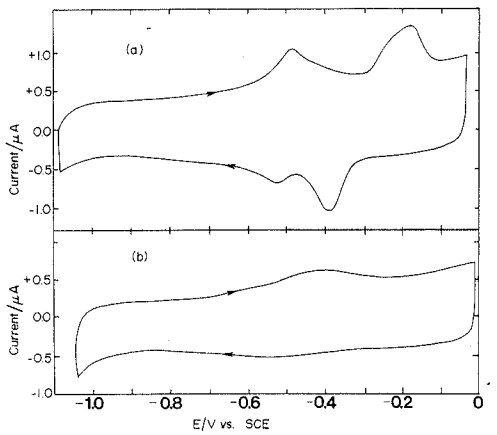

Fig. 1. (a) Typical cyclic voltammogram (continuous scan) for polycrystalline silver electrode (geometrical area = 0.0491 cm^2) at 0.1 V s^{-1} in 0.1 *M* NaF, following cyanide electropolishing (see text). (b) As in (a), but with additional pretreatment step involving soaking in 2 *M* $HClO_4$ (see text). Anodic current is plotted upward (positive sign).

The roughened silver electrodes were prepared by first mechanically polishing the electrode as above, and then were immersed in 0.1 *M* KCl while potentiostated at −0.1 V. The potential was then altered to 0.075 V, held there until 50 mC cm^{-2} of anodic charge had been passed, and then returned to −0.1 V and left until an essentially equal cathodic charge had accumulated. The electrode was then removed, rinsed with water, placed in 2 *M* $HClO_4$ for 20 min and subsequently immersed in 0.1 *M* NaF under potentiostatic control as described above for the smooth electrodes. This roughening procedure yields silver surfaces with roughness factors in the range ca. 2.5–5.0 as determined from anodic stripping of a upd lead monolayer; these surfaces exhibit intense SERS spectra for a variety of adsorbates [15].

RESULTS AND DISCUSSION

Capacitance measurements in sodium fluoride electrolytes

A number of authors [13,16–19] have reported differential capacitance–potential curves at polycrystalline silver electrodes in fluoride or perchlorate electrolytes. A comparison of the reported data shows reasonable agreement in the general features of the capacitance–potential curves; there being two maxima, one negative and one positive of the effective potential of zero charge (pzc) which is generally accepted to be in the vicinity of −0.95 V [12,13,17,18]. However, the potentials of the maxima are somewhat different in the various studies. Such differences may be attributed to the various pretreatments used which presumably yield differences in the surface inhomogeneity.

Figure 2 shows the concentration dependence of the differential capacitance C_m measured at a frequency of 1000 Hz at a polycrystalline silver electrode in aqueous

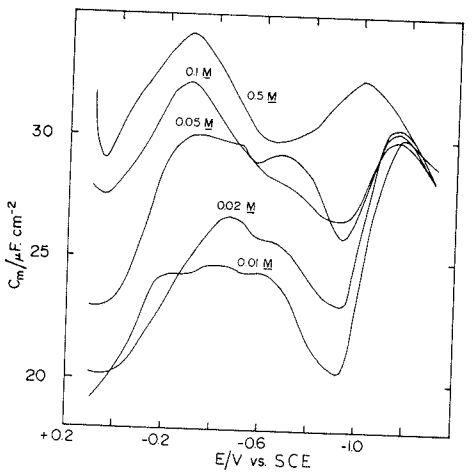

Fig. 2. Differential capacitance at 1000 Hz vs. electrode potential for polycrystalline silver in the various concentrations of sodium fluoride indicated.

sodium fluoride. The capacitance values varied significantly (±10%) between consecutive pretreatments, probably due to fluctuations in the surface area. They also exhibited a uniform time-dependent decrease over the whole potential range, possibly associated with some restructuring of the surface [16]. For these reasons the capacitance data shown are averages over several runs, the measurements being made within ca. 15 min after the silver electrode was introduced into the solution. The capacitance–potential curves show a number of features of interest. A clearly defined minimum develops in the capacitance–potential curves as the sodium fluoride concentration is decreased from 0.5 *M* to 0.01 *M*. The potential corresponding to this minimum, −0.93 V, changes insignificantly with varying concentration and occurs at a potential near those reported by Zelinskii and Bek [17] (−0.98 V), Sevast'yanov et al. [18] (−0.95 V) and Valette and Hamelin [13] (−0.97 V). The capacitance also decreases markedly as the solution concentration decreases at potentials positive of the minimum, suggesting that fluoride is specifically adsorbed under these conditions. Valette has recently concluded from capacitance data that fluoride is weakly specifically adsorbed at the (110) face at potentials positive of the pzc [21].

The frequency dependence of the capacitance for 0.02 *M* NaF at different potentials is illustrated in Fig. 3. At potentials more negative than −0.8 V the capacitance is (within 10%) independent of frequency between 1–1000 Hz, while at more positive potentials there is a marked increase of C_m apparent below 40 Hz. A similar trend can be seen in the data reported by Valette and Hamelin [13] (Fig. 21 of ref. 13): at 160 Hz, 120 Hz and 80 Hz their capacitance data appears frequency independent, while at 40 Hz there is a marked increase in the capacitance at potentials positive of the concentration-dependent minimum. This frequency dispersion could be associated with the adsorption of contaminants, or from interferences arising from slow faradaic processes.

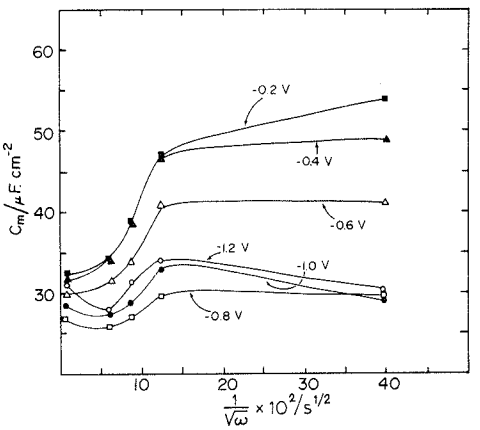

Fig. 3. Dependence of measured differential capacitance of polycrystalline silver in 0.02 *M* NaF upon $(\omega)^{-1/2}$, where ω is the angular frequency in radians s^{-1}.

There has recently been considerable discussion on the influence of surface inhomogeneity upon the double-layer structure at polycrystalline electrodes [12,13, 17,18]. Such surfaces are anticipated to contain "crystallite" regions consisting of the various low-index crystal planes, along with surface defects. A simplified treatment of the overall double-layer structure [12] indicates that the capacitance of the inner- and diffuse-layer regions can be coupled together in two different ways, depending on whether the surface region occupied by each crystal plane generates its own diffuse layer as well as inner layer, or whether each crystal plane generates a different inner layer, while maintaining a common diffuse layer across the entire surface. These alternatives have been termed Model I and Model II, respectively [12]. The simplest test of these models, at least in the absence of specific ionic adsorption, involves monitoring the dependence of the capacitance upon the ionic strength. Model II predicts behavior that is formally identical with the conventional Gouy–Chapman–Stern (GCS) model of a uniform (e.g. mercury) interface using an "effective" pzc that is a weighted mean of the pzc's for the individual crystal faces, depending on the relative contribution of each crystal face to the polycrystalline surface. However, Model I predicts ionic strength dependencies that are quite different from those of the GCS model [12].

Figure 4 consists of an analysis of the ionic strength dependence of C_m, expressed as "Parsons–Zobel" plots [22] of C_m^{-1} versus C_d^{-1}, where C_d is the diffuse-layer capacitance calculated from the Gouy–Chapman model, for a series of constant

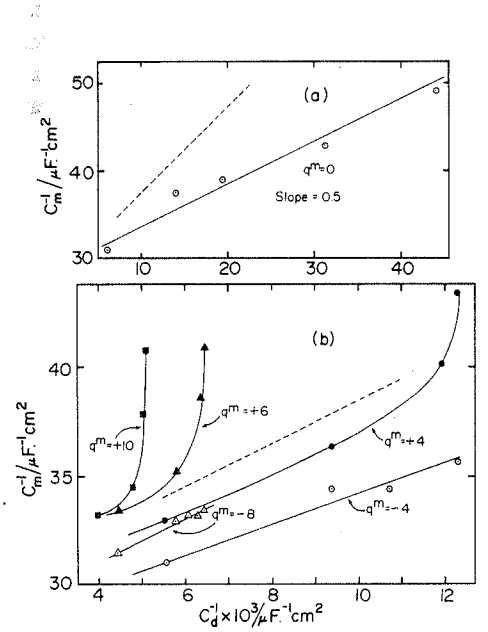

Fig. 4. Plots of the reciprocal of the measured differential capacitance against the reciprocal of the diffuse-layer capacitance calculated from Gouy–Chapman theory for several values of the electrode charge density q^m, using data taken from Fig. 2. The dashed lines have unit slopes.

excess electronic ("electrode") charge densities q^m. The values of q^m were estimated by integrating each capacitance curve in Fig. 2, assuming that the minimum in these curves (−0.93 V) constitutes the effective pzc. Figure 4(a) is such a plot for $q^m = 0$, and Fig. 4(b) contains plots for both positive and negative electrode charges. On the basis of Model II, the slope of these plots is expected to be 1/rf, whereas Model I predicts that smaller slopes will be obtained. Since rf ~ 1.2, the observed slope in Fig. 4(a) of 0.5 is consistent with Model I rather than Model II. Comparable results have been obtained previously [12]. This suggests that the dimensions of the individual crystallite regions are sufficiently large that the local variations of q^m expected between the different crystal faces yield corresponding local variations in the diffuse-layer structure. This result is not unexpected since Model II would only be expected to apply if the average crystallite size was comparable to, or smaller than, the diffuse-layer thickness ($\lesssim 3$ nm) for the ionic strengths employed in Fig. 4, which seems unlikely. Parsons–Zobel plots with non-unit slopes are also seen for both positive and negative values of q^m (Fig. 4(b)). The nonlinearities seen at positive electrode charges could well reflect the influence of fluoride specific adsorption; for increasing negative values of q^m the slopes approach the value of unity, as expected on the basis of either Model I or II if rf ~ 1.

Since the Model II does not apply to our results, the "average" pzc, E_{pzc}^{av}, (i.e. the electrode potential at which the net q^m for the overall surface equals zero) will, strictly speaking, differ from the electrode potential corresponding to the measured capacitance minimum E_{min} in dilute electrolytes [12]. However, it seems likely that $E_{pzc}^{av} \sim E_{min}$ for this system. Thus E_{min} remains essentially constant (within ca. 10 mV) as the ionic strength increases; significant variations in E_{min} would be expected if E_{pzc}^{av} and E_{min} were greatly different [12]. Of the various low index crystal faces of silver, the (111) faces have a p.z.c. in fluoride media of −0.68 V, whereas the (100) and (110) faces exhibit p.z.c. values of −0.91 V and −0.98 V, respectively [13]. The (210) face has been reported to have a pzc in fluoride media which is 0.03 V more negative than the (110) face [7]. Approximate calculations on the basis of Model I predict that a significant capacitance minimum should appear in dilute electrolytes in the vicinity of −0.68 V if (111) crystallites form a large (say $\gtrsim 20\%$) contribution to the polycrystalline surface. The absence of such a minimum, and the presence of a single minimum for polycrystalline silver in the potential region (−0.09 V to −1.0 V) where the pzc for the (100), (110), and (210) faces occur, suggest that the polycrystalline surface may well be a composite of crystallites for these and higher order crystal faces, along with the inevitable surface defects. It is interesting to note that the pzc values for the various crystal faces follow the same sequence as the crystallographic packing densities which decrease in the order (111) > (100) > (110) > (210) [21]. It seems reasonable that the relative randomness of the polycrystalline surface would favor crystallites with lower atomic packing densities, with pzc values clustered closely around −0.95 V.

Anion specific adsorption from capacitance measurements

(i) Chloride

Figure 5 shows capacitance–potential curves obtained at 1000 Hz for solutions containing sodium fluoride and chloride concentrations varying from 45 μM to 17 mM, each having a total ionic strength $\mu = 0.5$. In order to correct for the time dependence of the capacitance discussed earlier the capacitance–potential curves were normalized to a constant value at -1.2 V vs. SCE; the capacitance was found to be almost independent of chloride concentration at this and more negative potentials. At low chloride concentrations (< 3.9 mM) two peaks, at -0.7 V (A) and -0.2 to -0.3 V (B) are observed in the capacitance curves, while at higher concentrations A becomes a shoulder on peak B. The capacitance–potential curves for chloride-containing solutions at the various low index crystal planes have been found to exhibit several characteristic maxima [7]. The (111) face yield a large maximum at ca. -0.6 to -0.7 V; this may be responsible for the minor peak A in Fig. 5. The major peak B in Fig. 5 possibly arises from chloride adsorption on other low index faces; the (110) and (100) surfaces both yield large maxima in chloride solutions in this region [7].

The surface concentrations Γ_x' of specifically adsorbed chloride, as well as the other anions in this study, were calculated from such capacitance–potential curves by using a modified version of the "Hurwitz–Parsons" analysis [23] described by

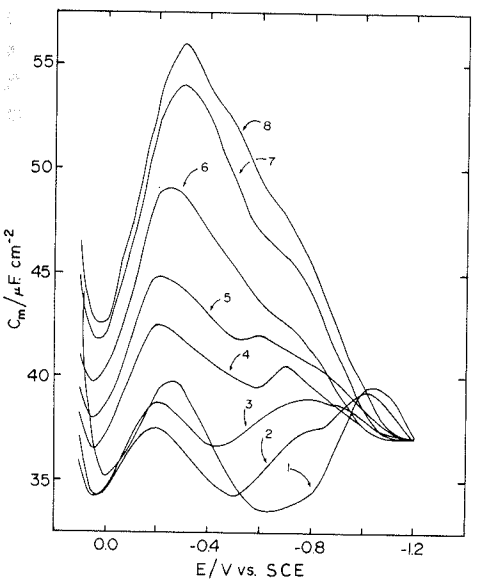

Fig. 5. Differential capacitance at 1000 Hz vs. electrode potential for polycrystalline silver in mixed NaF/NaCl electrolytes at an ionic strength of 0.5 M. Chloride concentrations: (1) 0; (2) 4.5 μM; (3) 0.18 mM; (4) 0.75 mM; (5) 1.2 mM; (6) 3.9 mM; (7) 11 mM; (8) 17 mM.

Weaver and Anson [24]. This method utilizes the equation

$$\Gamma'_x = -(\Delta q^m)_E / RT(\partial \ln c_b / \partial E)_{\Gamma'_x} \quad (1)$$

where $(\Delta q^m)_E$ is the difference in the average excess electronic charge density at the electrode between the 0.5 M NaF base electrolyte and a given chloride-containing solution at a given electrode potential E. This quantity was found from the displacement in the corresponding electrode charge–potential curves for the various solution compositions. These curves were obtained by integrating the capacitance–potential data from a sufficiently negative potential where the capacitance, and presumably therefore the electrode charge density q^m, is unaltered upon the addition of the adsorbing species to the bulk solution [24]. The coefficient $RT(\partial \ln c_b/\partial E)_{\Gamma'_x}$ was found by analyzing the shapes of these charge–potential curves using the procedure described in ref. [24]. This quantity is closely related to the so-called "electrosorption valency" [25] $(RT/F)(\partial \ln c_b/\partial E)_{\Gamma'_x}$. Although the values of the electrosorption valency (EV) were roughly ($\sim \pm 20\%$) independent of Γ'_{Cl^-}, they decreased significantly with decreasing negative electrode potential; for example, at -0.9 V, EV = 0.25; at -0.3 V, EV ~ 0.15.

Figure 6 contains the resulting plots of Γ'_{Cl^-} against electrode potential for each bulk chloride concentration c_b. By assuming that the average pzc equals -0.93 V, these values of Γ'_{Cl^-} can also be plotted against the average electrode charge density q^m, as shown in Fig. 7.

The dependence of Γ'_{Cl^-} upon c_b was analyzed at various constant electrode

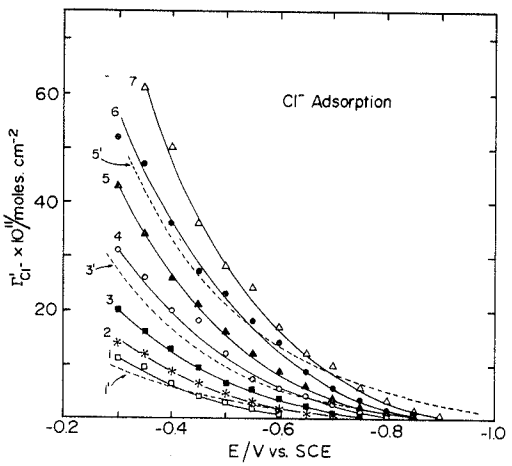

Fig. 6. The concentration of specifically adsorbed chloride Γ'_{Cl^-} plotted against electrode potential for the following bulk chloride concentrations: (1) 0.18 mM; (2) 0.75 mM; (3) 1.6 mM; (4) 3.9 mM; (5) 7.6 mM; (6) 11 mM; (7) 17 mM. The curves 1′, 3′ and 5′ are those obtained for 0.2, 1.6, and 8 mM bulk chloride, respectively, after electrochemical roughening of the silver surface. Roughness factor rf ~ 4 (see text).

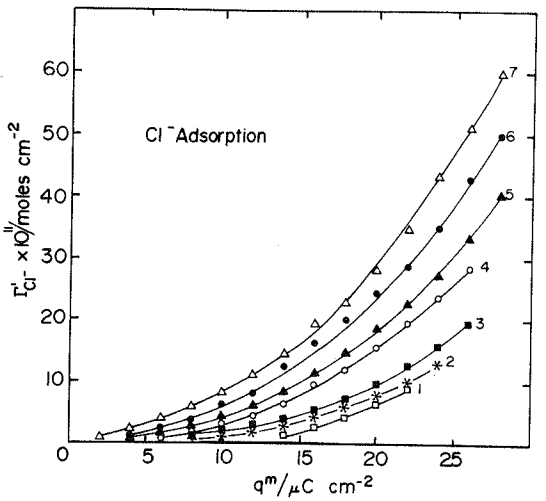

Fig. 7. As for Fig. 6, but Γ'_{Cl^-} plotted against the electrode charge density q^m.

charges q^m using a Frumkin isotherm. This can be written in the form

$$(c_b/c_o)\exp(-\Delta G_a^0/RT) = (\Gamma_s/\Gamma_o)[\theta/(1-\theta)]\exp(g\theta) \tag{2}$$

where Γ_s is the surface concentration corresponding to a monolayer coverage, c_o and Γ_o are the standard state concentrations for the adsorbing species in the bulk and at the surface, respectively, θ is the fractional coverage ($=\Gamma'_x/\Gamma_s$), g is a surface interaction parameter, and ΔG_a^0 is the standard free energy of adsorption. Plots of $\ln c_b - \ln[\theta/(1-\theta)]$ against θ were drawn in order to determine the interaction parameter g from the slope, and ΔG_a^0 from the intercept. The maximum surface concentration Γ_s of chloride ions is estimated to be 1.6×10^{-9} mol cm^{-2}, assuming the ionic radius to be 0.18 nm [26]. Illustrative values of ΔG_a^0 for chloride, at $q^m = 0$ and $+15\ \mu$C cm^{-2}, obtained from the adsorption data in Fig. 7 are given in Table 1. (The surface and bulk standard states, Γ_o, employed are the conventional values of 1 molecule cm^{-2} and 1 mol l^{-1}, respectively, both referring to infinite dilution [Henry's Law] in the 0.5 M NaF base electrolyte employed here.) Positive values of g were obtained, in the range ca. 5–10 for values of q^m in the range 10–30 μC cm^{-2}, indicating repulsive interactions between the adsorbed chloride ions. The plots are decidedly nonlinear for small θ at large values of q^m, most probably due to co-adsorption of fluoride ions.

Measurements of differential capacitance against electrode potential in mixed fluoride–chloride electrolytes at polycrystalline silver have also been reported by Shlepakov and Sevast'yanov [8] and by Fleischmann et al [19]. In the latter paper, noticeably greater increases in C_m are reported upon the addition of chloride than were observed in the present work (Fig. 5). Although the ionic strength was not maintained constant and no adsorption analysis was given [19], these data yield

TABLE 1

Standard free energies of adsorption ΔG_a^0 for several anions at silver and mercury electrodes

Electrode	Adsorbate	Adsorption Free Energy $-\Delta G_a^0$/kJ mol^{-1} [a]	
		$q^m = 0$	$q^m = 15\ \mu C\ cm^{-2}$
Polycrystalline silver	Cl^- (0.5 *M* NaF)	83 [b]	95 [b]
Polycrystalline silver	Cl^- (0.1 *M* NaF)	86 [b]	
Polycrystalline silver	Cl^- (0.1 *M* $NaClO_4$)		(104)
(111) Silver	Cl^- (0.04 *M* NaF)	100 [c]	
(100) Silver	Cl^- (0.04 *M* NaF)	95 [c]	
(100) Silver	Cl^- (0.04 *M* NaF)	93 [c]	
Polycrystalline silver	Br^- (0.5 *M* NaF)	96 [b]	104 [b]
Polycrystalline silver	Br^- (0.1 *M* $NaClO_4$)		(114)
Polycrystalline silver	N_3^- (0.5 *M* NaF)	93 [b]	
	NCS^- (0.1 *M* $NaClO_4$)		(115)
Mercury	Cl^- (1 *M* KF)	82 [d]	
	Br^- (1 *M* KF)	90 [e]	
	N_3^- (0.95 *M* NaF)	86 [f]	

[a] Obtained by extrapolating adsorption data obtained from capacitance measurements to zero coverage using eqn. (2) unless where noted (see text). Values in parentheses obtained from kinetic probe data (see text). Standard states are 1 molecule cm^{-2} for the adsorbate, and 1 mol l^{-1} for the bulk solution.
[b] From data obtained in present work.
[c] From ref. 7, obtained from data extrapolation using virial isotherm.
[d] From data given in ref. 33.
[e] From data given in ref. 29.
[f] From data given in ref. 34.

chloride surface concentrations that are up to ten fold larger at comparable electrode potentials and bulk chloride concentrations then given in Fig. 6. Significantly (2–3 fold) greater amounts of chloride adsorption are also obtained from an analysis of the capacitance–potential data given in ref. [8]. In order to ascertain whether these disparities arise from true differences in the extent of chloride adsorption or partly from experimental artifacts, the dependence of C_m upon the ac frequency in the range 20–1500 Hz was investigated for several of the solution compositions in Fig. 5. Significant increases in C_m were found with decreasing frequency at potentials positive of -0.8 V, similar to that shown in Fig. 3. However, this frequency dependence was only slightly greater for the chloride-containing solutions, so that the apparent concentrations of adsorbed chloride calculated using the above analysis only increased marginally using the data gathered at smaller frequencies (typically a 50% increase in Γ'_{Cl^-} as the frequency was altered from 1000 to 40 Hz). This result indicates that adsorption–desorption equilibrium is maintained throughout the a.c. potential excursion. The use of high frequencies is inadvisable for low bulk concentrations of adsorbate since it is likely that adsorption–desorption equilibrium will

not be entirely maintained throughout the ac cycle as a consequence of diffusion polarization. However, the frequency dependence of the capacitance was found to be approximately independent of the chloride bulk concentration at least down to ca. 0.1 mM, indicating that this effect is unimportant under these conditions, as is required for the thermodynamic analysis to be valid.

Some experiments were run at a frequency of 40 Hz using 0.1 M NaF as the base electrolyte in order to reproduce the measurement conditions of ref. 19 and to check if this lower ionic strength used in ref. 19 had an important bearing on the results. Roughly 2 to 2.5-fold greater amounts of chloride adsorption were determined in 0.1 M NaF compared with corresponding conditions in 0.5 M NaF. These differences may be due to a greater extent of fluoride specific adsorption at the larger ionic strength, thereby diminishing the availability of surface sites for chloride specific adsorption. However, the extent of chloride adsorption was still noticeably (3–4 fold) less in our experiments compared to that obtained from the data in ref. 18. It therefore seems likely that an important reason for these disparities lies in structural differences between the polycrystalline surfaces prepared here and by Fleischmann et al. [19]. A chemical polishing procedure was used in ref. 19; although we have previously employed such a pretreatment, in our hands the electropolishing method used here was found to yield more reproducible surfaces.

Capacitance–potential curves were also obtained in chloride-containing solutions at anodically roughened silver surfaces, prepared as described in the Experimental section. Analysis of these data yielded values of Γ'_{Cl^-} once corrected for the roughness factor, that are surprisingly close (within ca. 50%) of those for "smooth" electrodes at a given electrode potential and bulk chloride concentration. Some typical data are shown as dashed lines in Fig. 6. Further results for chloride and other anionic adsorbates will be described in detail elsewhere [27].

(ii) Bromide

The adsorption of bromide at various single crystal silver faces has been previously reported [7], although no quantitative analysis of bromide specific adsorption has been undertaken. Figure 8 shows capacitance–potential curves obtained at 1000 Hz for polycrystalline silver in solutions of ionic strength $\mu = 0.5\,M$ containing sodium fluoride and added sodium bromide having concentrations in the range 0.04–14.5 mM. It is seen that the capacitance–potential curves have similar shapes as those for chloride although shifted to more negative potentials. Figure 8 also includes the resistive component R_m plotted as a function of potential for 4.0 mM Br^-, shown as a dashed line. At potentials positive of -0.7 V, R_m increases and goes through a maximum at -0.4 V. Since linear sweep voltammograms do not show any significant anodic faradaic current in this potential range, this effect is unlikely to be due to silver dissolution. This variation in R_m was found to become more pronounced and the potential at which the maximum occurred shifted to more negative values as the bromide concentration was increased and the ac frequency was decreased. The origin of the latter effect is unclear, although it does appear to be associated with substantial quantities of ionic adsorption. Consequently, the adsorp-

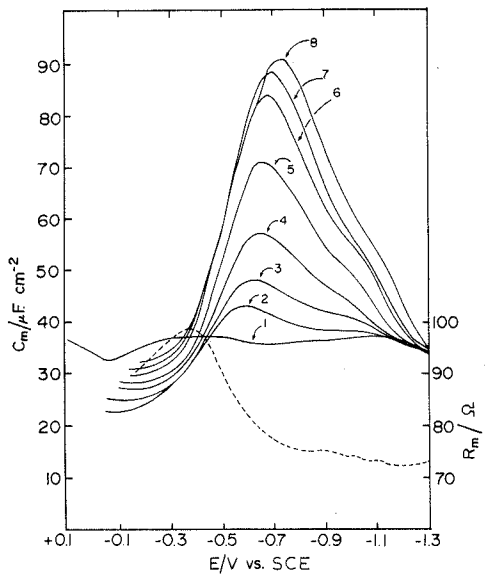

Fig. 8. Differential capacitance at 1000 Hz vs. electrode potential of polycrystalline silver (———) in mixed NaF/NaBr electrolytes at an ionic strength of 0.5 *M*. Bromide concentrations: (1) 0; (2) 0.04 m*M*; (3) 0.15 m*M*; (4) 0.36 m*M*; (5) 0.88 m*M*; (6) 1.93 m*M*; (7) 4.0 m*M*; (8) 14.5 m*M*. (— — —) Resistive component R_m for 4.0 m*M* Br^- plotted on the same potential scale.

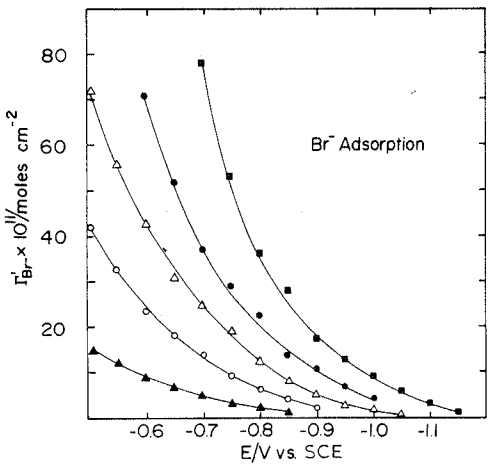

Fig. 9. The concentration of specifically adsorbed bromide Γ'_{Br^-} plotted against the electrode potential for the following bulk bromide concentrations: (1) 0.04 m*M*; (2) 0.15 m*M*; (3) 0.36 m*M*; (4) 0.88 m*M*; (5) 1.9 m*M*.

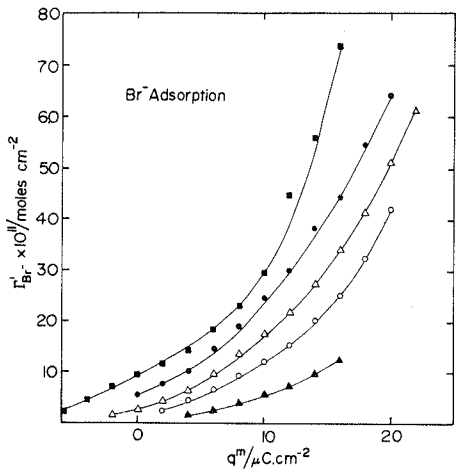

Fig. 10. As for Fig. 9, but Γ'_{Br^-} plotted against the electrode charge density q^m.

tion analysis for this and other systems was restricted to potentials where the resistive component was invariant; under these conditions the capacitance component was also found to be essentially independent of frequency (cf. chloride above).

The plots of the surface concentration of specifically adsorbed bromide Γ'_{Br^-} versus electrode potential and electrode charge density, obtained from the capacitance data in Fig. 8, are shown in Figs. 9 and 10, respectively. As for chloride, the electrosorption valencies tended to decrease with decreasing negative electrode potential; for example at -0.9 V, EV $= 0.35$; at -0.6 V, EV $= 0.2$. Plots of $\ln c_b - \ln(\theta/1-\theta)$ versus θ at various electrode charges were again used to extract adsorption parameters [eqn. (2)]. The maximum surface concentration of bromide ions is estimated to be 1.35×10^{-9} mol cm^{-2}, assuming the ionic radius to be 0.197 nm [26]. Reasonably linear plots were obtained for q^m in the range 0–20 μC cm^{-2} with values of g ranging from 15 (at $q^m = 0$) to 10 (at $q^m = 20\mu$C cm^{-2}). Values of ΔG_a^0 derived from the plots of $q^m = 0$ and 15 μC cm^{-2} are given in Table 1. Similarly large values of g (e.g., 14 at $q^m = 8$ μC cm^{-2}) are also obtained by plotting the corresponding data for bromide adsorption at mercury electrodes [29] in the same manner.

(iii) Iodide

Figure 11 shows capacitance–potential curves for polycrystalline silver in 0.5 M sodium fluoride with five concentrations of iodide added in the range 40 μM to 1.85 mM. The general shape of the curves is similar to that observed for chloride and bromide, but with a sharp capacitance maximum at -1.1 V, and a striking depression of the capacitance to values around 15 μF cm^2 at potentials more positive than -0.8 V. These characteristics are similar to those found at the various low-index single crystal faces [7,28]. The behavior of the resistive component of the cell

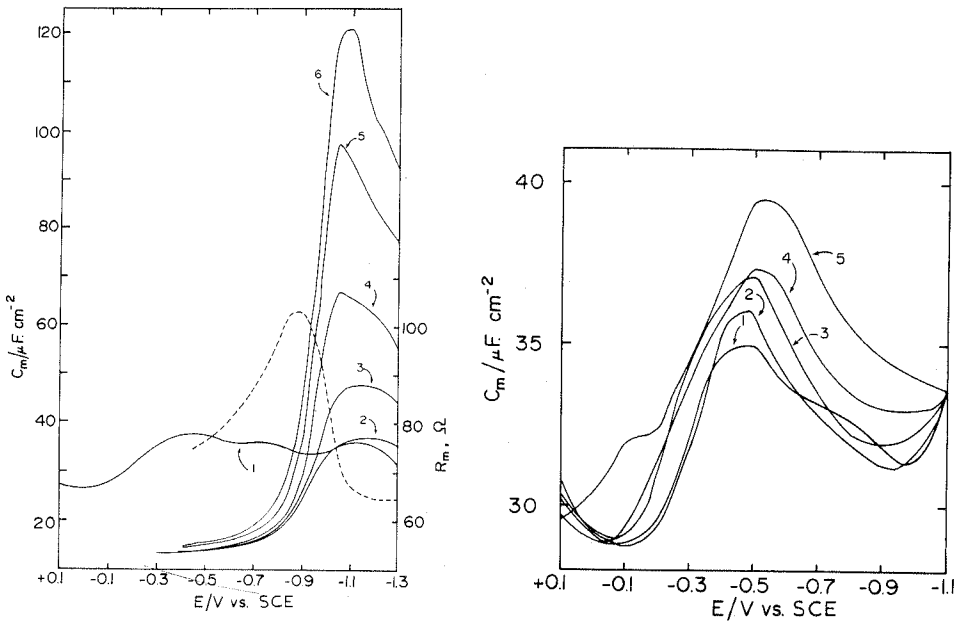

Fig. 11. Differential capacitance at 1000 Hz vs. electrode potential of polycrystalline silver (———) in various mixed NaF/NaI electrolytes at an ionic strength of 0.5 *M*. Iodide concentrations: (1) 0; (2) 0.04 m*M*; (3) 0.14 m*M*; (4) 0.36 m*M*; (5) 0.84 m*M*; (6) 1.85 m*M*. (— — —) Resistive component for 0.84 m*M* I^- plotted on the same potential scale.

Fig. 12. Differential capacitance at 1000 Hz vs. electrode potential of polycrystalline silver in mixed NaF/NaN_3 electrolytes at an ionic strength of 0.5 *M*. Azide concentrations: (1) 0; (2) 0.02 m*M*; (3) 0.1 m*M*; (4) 0.28 m*M*; (5) 0.9 m*M*.

impedance as a function of electrode potential is also shown for the 0.84 m*M* iodide solution as a dashed line in Fig. 11. As for bromide, it is seen that the resistive component exhibits a pronounced maximum in the same potential region (ca. −0.8 V) as the capacitive component falls to a small constant value.

Unfortunately, it was not possible to extract the extent of specific iodide adsorption from a Hurwitz–Parsons analysis of the capacitance–potential curves since large capacitance increases were observed upon iodide addition even at the most negative potentials (ca. −1.3 V) for which data could be obtained without interference from hydrogen evolution. Qualitatively, however, it appears that iodide is much more strongly adsorbed than are chloride and bromide.

(iv) Azide

Figure 12 shows capacitance–potential curves obtained in solutions containing from 22 μM to 0.9 m*M* sodium azide maintained at $\mu = 0.5\,M$ using sodium fluoride. At higher azide concentrations the capacitance increased significantly even

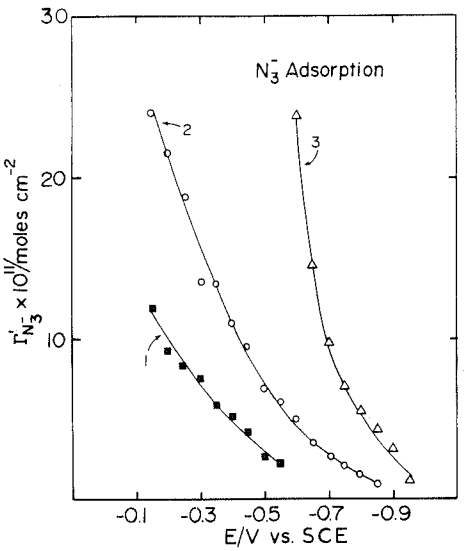

Fig. 13. The concentration of specifically adsorbed azide $\Gamma'_{N_3^-}$ plotted against electrode potential for the following bulk azide concentrations: (1) 0.1 mM; (2) 0.28 mM; (3) 0.9 mM.

at the most negative potentials so that the adsorption analysis was limited to a fairly narrow concentration range. The resulting plots of the azide surface concentration $\Gamma'_{N_3^-}$ against the electrode potential and electrode charge density are shown in Figs. 13 and 14, respectively. An approximate estimate of ΔG_a^0 at $q^m = 0$ derived from Fig. 14 using eqn. (2) is given in Table 1.

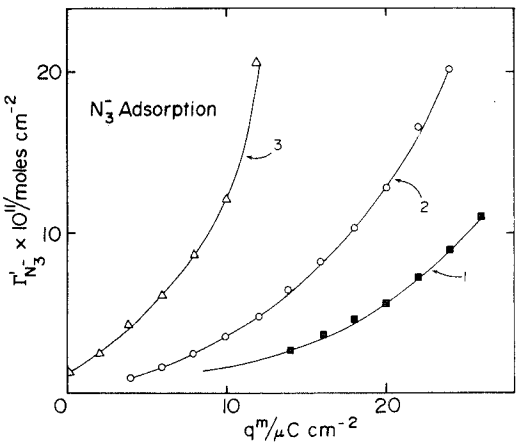

Fig. 14. As for Fig. 13, but $\Gamma'_{N_3^-}$ plotted against the electrode charge density q^m.

(v) Thiocyanate

Figure 15 shows capacitance–potential curves obtained in 0.5 *M* NaF with the addition of between 0.3 and 30 m*M* of thiocyanate. As for iodide, it is seen that very small concentrations of thiocyanate have a profound effect upon the capacitance–potential behavior. Again, quantitative determination of the extent of adsorption is precluded by the inability to measure the capacitance at a sufficiently negative potential so that thiocyanate is not significantly adsorbed. Nevertheless, as for iodide it is evident that thiocyanate is strongly adsorbed even at negative potentials (beyond −1.0 V) and small bulk concentrations of thiocyanate. The overall shape of the capacitance–potential curves differs from those for the halides in that two pronounced capacitance peaks are observed, at ca. −1.1 and −0.6 V. Since the second peak occurs within a potential range where the thiocyanate coverage approaches saturation, it seems plausible that it may be due to a change of the adsorbate structure. Recent measurements of SERS for thiocyanate at mildly roughened silver electrodes provide some support to this notion; these results will be discussed in detail elsewhere [30].

An unusual aspect of the thiocyanate system is that in the potential range ca. −0.9 V to −1.1 V constant capacitance values were only obtained after ca. 2–5 min following large potential excursions. Normally, the capacitance values at silver responded rapidly and reversibly to changes in either the bulk anion concentration or the electrode potential.

Anion specific adsorption from kinetic probe measurements

Although the differential capacitance measurements described above are expected to provide relatively accurate estimates of the extent of ionic specific adsorption at

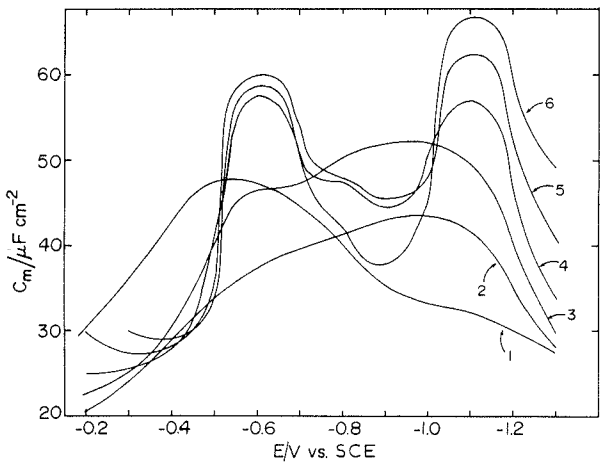

Fig. 15. Differential capacitance at 1000 Hz vs. electrode potential for polycrystalline silver in mixed NaF/NaNCS electrolytes at an ionic strength of 0.5 *M*. Thiocyanate concentrations: (1) 0; (2) 0.3 m*M*; (3) 1.0 m*M*; (4) 3.0 m*M*; (5) 10 m*M*; (6) 30 m*M*.

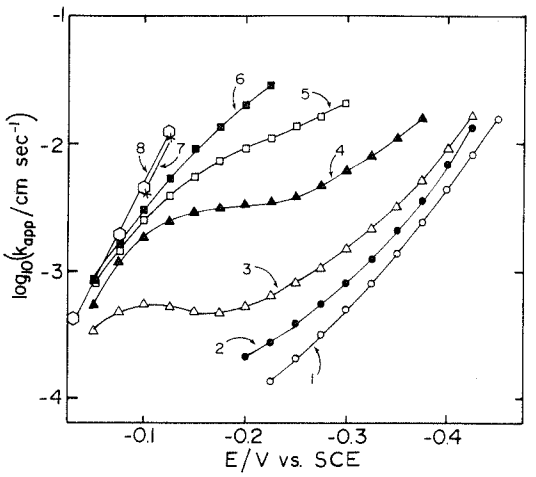

Fig. 16. Plots of the logarithm of the apparent rate constant for the reduction of $Co(NH_3)_5F^{2+}$ at a polycrystalline silver electrode in 0.1 M $NaClO_4$ + 2 mM $HClO_4$, against the electrode potential, with the following additions of NaCl: (1) 0; (2) 2 μM; (3) 5 μM; (4) 20 μM; (5) 50 μM; (6) 100 μM; (7) 1 mM; (8) 10 mM.

solid as well as liquid metal surfaces, the method has some inherent limitations. Thus the data analysis could not be employed for anions such as thiocyanate or iodide that are adsorbed even at the most negative potentials. Also, the technique is subject to the usual limitations of capacitance measurements at solid electrodes arising from frequency dispersion effects, etc.

We have recently pointed out that useful semiquantitative estimates of the extent of specific ionic adsorption at silver electrodes may be obtained using the outer-sphere reduction of suitable Co(III) complexes, especially $Co(NH_3)_6^{3+}$ and $Co(NH_3)_5F^{2+}$, as "kinetic probes" [1,31]. These reactions are especially suitable on account of the sensitivity of their reduction kinetics to the diffuse-layer composition and the close adherence of such double-layer effects to the predictions of the simple Gouy–Chapman–Stern–Frumkin (GCSF) model [31,32].

Figure 16 contains some typical kinetic data for $Co(NH_3)_5F^{2+}$ reduction at polycrystalline silver in 0.1 M $NaClO_4$ + 2 mM $HClO_4$ and with the addition of varying amounts of chloride in the range 1.0 μM to 10 mM. It is seen that striking rate increases (up to ca. three orders of magnitude) are obtained upon the addition of chloride ions, as expected since an increase in anion specific adsorption will substantially enhance the concentration of the cationic reactant at the reaction plane. Also, it is interesting to note that for $E > -0.15$ V, the values of k_{app} no longer increase with further additions of chloride above about 0.5 mM. This point may correspond to concentrations of specifically adsorbed chloride that approach a monolayer, although it may simply arise from a "rate saturation" effect due to the very large (> 1 M) interfacial reactant concentrations that are produced under these

conditions. The changes in the logarithm of the apparent rate constant k_{app} at a given electrode potential, $(\Delta \log k_{app})_E$, can be related to the change in the potential at the reaction plane, $\Delta\phi_{rp}^E$, by [31,32]

$$(\Delta \log k_{app})_E = -(F/2.303RT)(z_r - \alpha)\,\Delta\phi_{rp}^E \tag{3}$$

where z_r is the charge number of the reactant, and α is the electrochemical transfer coefficient. Using Gouy–Chapman theory, the quantity $\Delta\phi_{rp}^E$ can in turn be related to the corresponding change in the charge density residing inside the o.H.p., $\Delta(q^m + q'_x)_E$, where q'_x $(= -F\Gamma'_x)$ is the charge density due to specifically adsorbed anions. A drawback of this approach therefore is that the kinetic response is partly determined by the alteration of the electrode charge, $(\Delta q^m)_E$, brought about by anion specific adsorption. However, the relative values of $(\Delta q^m)_E$ and q'_x can be determined from the electrosorption valency since from eqn. (1), $(\partial q^m/\partial q'_x)_E = (\partial q^m/F\,\partial\Gamma'_x)_E = -(RT/F)(\partial \ln c_b/\partial E)_{\Gamma'_x}$; this coefficient is relatively small (ca. 0.2–0.35) at silver for the conditions employed here.

The experimental values of $(\Delta \log k_{app})_E$ found for various additions of chloride (Fig. 16) can be used to estimate values of $\Delta\phi_{rp}^E$ and hence q'_{Cl^-} in this manner. Since the proportionality constant between $\Delta\phi_{rp}^E$ and q'_{Cl^-} depends somewhat upon the absolute values of the net charge density inside the o.H.p., $(q^m + q')_E$, rough estimates of this quantity in the absence of chloride adsorption are required. Although q^m is large and positive (ca. 15–20 μC cm^{-2}) in the potential region over which the kinetic data were gathered (ca. -0.2 V to -0.4 V) this is approximately offset by the charge due to specifically adsorbed perchlorate anions in 0.1 *M* $NaClO_4$, so that $(q^m + q')_E \sim 0$ [1,2].

A virtue of the kinetic probe method is that it can be extremely sensitive to small amounts of specific adsorption from added ions. For example, for the reduction of $Co(NH_3)_6^{3+}$ in 0.1 *M* electrolyte a two-fold rate change corresponds to a value of $\Delta(q^m + q')_E$ of as little as 0.5 μC cm^{-2}, corresponding to $\Gamma'_x \sim 5 \times 10^{-12}$ mol cm^{-2}. Since reasonable adherence to Henry's Law (i.e. proportionally between Γ'_x and c_b) is expected at such very small coverages, approximate estimates of ΔG_a^0 for chloride can be obtained in this manner using the expression

$$\Delta G_a^0 = -RT\left[\ln\left(\Gamma'_x/\text{molecules cm}^{-2}\right) - \ln\left(c_b/\text{mol l}^{-1}\right)\right] \tag{4}$$

A representative value of ΔG_a^0 for chloride, obtained at $q^m = +15$ μC cm^{-2} ($\equiv -0.4$ V vs. SCE) is listed in Table 1. Values of ΔG_a^0 are also given from bromide and thiocyanate adsorption at $q^m = 15$ μC cm^{-2} that were obtained from kinetic probe data in the same fashion. Comparison with the corresponding values of ΔG_a^0 obtained for chloride and bromide at $+15$ μC cm^{-2} from the capacitance measurements (Table 1) shows that the kinetic probe estimates are about 10 kJ mol^{-1} more negative. These disparities are probably due, at least in part, to the differences in the extent of perchlorate and fluoride specific adsorption from the base electrolytes employed for the kinetic probe and capacitance measurements. Also, the kinetic probe technique may respond preferentially to regions of the surface inducing the greatest increases in the extent of anion adsorption, yielding apparently more

negative values of ΔG_a^0 than using the capacitance technique which reflects the *average* extent of adsorption for the entire surface.

The reduction kinetics of $Co(NH_3)_5F^{2+}$ in 0.1 *M* KPF_6, 0.1 *M* $NaClO_4$, and 0.1 *M* NaF at −300 mV exhibit values of log k_{app} in the order of $F^- > ClO_4^- > PF_6^-$, which from eqn. (3) yields small yet significant ($\lesssim 4 \times 10^{-11}$ mol cm^{-2}) differences in the extent of specific anion adsorption in this sequence. Such an order has been noted recently by Valette [21].

Comparison between adsorption free energies for various anions

Table 1 contains a comparison of standard free energies of adsorption ΔG_a^0 at the pzc for chloride, bromide, and azide obtained from capacitance measurements in the present work with values of ΔG_a^0 for chloride at various single crystal silver surfaces; and for chloride, bromide, and azide at mercury electrodes obtained using similar base electrolytes (≈ 1 *M* fluoride). The latter values were extracted from literature data [29,33,34]. It is seen that the (100) and (110) single crystal faces, although having pzc values close to (within ca. 0.05 V) of the effective pzc of the polycrystalline surface, yield values of ΔG_a^0 for chloride adsorption that are noticeably more negative. Part of this difference may be due to the markedly smaller fluoride concentrations used in the single crystal study; indeed, the value of ΔG_a^0 obtained here in 0.1 *M* NaF is significantly more negative than that for 0.5 *M* NaF (Table 1).

Comparison between the values of ΔG_a^0 at polycrystalline silver and mercury indicates that the substantially more favorable thermodynamics for chloride adsorption at a given electrode potential at the former surface arises primarily from its markedly more negative pzc. However, significant differences between polycrystalline silver and mercury are also seen at the pzc. At silver the values of ΔG_a^0 for azide and bromide are 10 and 13 kJ mol^{-1} more negative than for chloride in 0.5 *M* NaF, whereas at mercury the corresponding variations in ΔG_a^0 are only −4 and −8 kJ mol^{-1}. These behavorial differences may reflect a greater tendency of silver to stabilize the specifically adsorbed state by means of overlap of the electron pair on the adsorbing anions with the metal surface orbitals. Such electron sharing is expected to be greater for bromide and azide relative to chloride, and to a greater extent at silver than at mercury as a result of the higher electron affinity of the former metal [35]. However, larger increases in $-\Delta G_a^0$ for bromide versus chloride at silver compared to those at mercury are also predicted on the basis of a purely electrostatic model [36]. The electrosorption valencies found here for chloride and bromide at silver in the vicinity of the pzc (ca. 0.25 and 0.35, respectively) are markedly smaller than the estimates (ca. 1.0) given previously [37], based on an analysis of adsorption data obtained using a thin-layer technique [10]. The present smaller values seem more reliable since the Hurwitz–Parsons analysis provides a particularly direct route to the electrosorption valency. Small fractional values, EV ≈ 0.2–0.3, are indeed predicted for chloride and bromide at silver on the basis of electronegativity differences (Fig. 2 of ref. 37). The present values are close to the corresponding quantities at mercury (ca. 0.2 and 0.35, respectively, at high ionic

strengths [24,37]), supporting the view that the anion–silver bonds are predominantly ionic under these conditions.

ACKNOWLEDGMENT

This work is supported by the Air Force Office of Scientific Research.

REFERENCES

1 K.L. Guyer, S.W. Barr and M.J. Weaver in S. Bruckenstein, J.D.E. McIntyre and B. Miller (Eds.), Proceedings 3rd Symposium on Electrode Processes, The Electrochemical Society, Princeton, NJ, 1980, p. 390.
2 S.W. Barr, K.L. Guyer and M.J. Weaver, J. Electroanal. Chem., 111 (1980) 41.
3 M.J. Weaver, Inorg. Chem., 18 (1979) 402.
4 K.L. Guyer, S.W. Barr and M.J. Weaver, in W.E. O'Grady, P.N. Ross, Jr. and F.G. Wills (Eds.), Proceedings Symposium on Electrocatalysis, Electrochemical Society, Pennington, NJ, 1982, p. 377.
5 K.L. Guyer and M.J. Weaver, J. Am. Chem. Soc., submitted.
6 For reviews, see R.P. van Duyne in C.B. Moore (Ed.), Chemical and Biochemical Applications of Lasers, Vol. 4, Academic Press, New York, 1978, Ch. 4; T.E. Furtak and J. Reyes, Surf. Sci., 93 (1980) 351.
7 G. Valette, A. Hamelin and R. Parsons, Z. Phys. Chem. N.F., 113 (1978) 71.
8 A.V. Shlepakov and E.S. Sevast'yanov, Sov. Electrochem., 14 (1978) 243.
9 W. Paik, M.A. Genshaw and J.O'M. Bockris, J. Phys. Chem., 74 (1970) 4266.
10 E. Schmidt and S. Stucki, Ber. Bunsenges. Phys. Chem., 77 (1973) 913; E. Schmidt and S. Stucki, J. Electroanal. Chem., 43 (1973) 425.
11 R.E. Kunz, J.G. Gordon II, M.R. Philpott and A. Girlando, J. Electroanal. Chem., 112 (1980) 391; R.P. Cooney, E.S. Reid, M. Fleischmann and P.J. Hendra, J. Chem. Soc. Faraday Trans. 1, 73 (1977) 1691; H.S. Gold and R.P. Buck, J. Raman Spectrosc., 8 (1979) 323; H. Wetzel, H. Gerischer and B. Pettinger, Chem. Phys. Lett., 80 (1981) 159.
12 I.A. Bagotskaya, B.B. Damaskin and M.D. Levi, J. Electroanal. Chem., 115 (1980) 189.
13 G. Valette and A. Hamelin, J. Electroanal. Chem., 45 (1973) 301.
14 J.T. Hupp, D. Larkin, H.Y. Liu and M.J. Weaver, J. Electroanal. Chem., 131 (1982) 299.
15 K.L. Guyer, Ph.D. Thesis, Michigan State University, 1981.
16 N.A. Hampson, D. Larkin and J.R. Morley, J. Electrochem. Soc., 114 (1967) 817.
17 A.G. Zelinskii and R.Yu. Beck, Sov. Electrochem., 14 (1978) 1583.
18 E.S. Sevast'yanov, M.N. Ter-Akopyan and V.K. Chubarova, Sov. Electrochem., 16 (1980) 368.
19 M. Fleischmann, J. Robinson and R. Waser, J. Electroanal. Chem., 117 (1981) 257.
20 D.C. Grahame, J. Am. Chem. Soc., 76 (1954) 4819.
21 G. Valette, J. Electroanal. Chem., 122 (1981) 285.
22 R. Parsons and F.G.R. Zobel, J. Electroanal. Chem., 9 (1965) 333.
23 H.D. Hurwitz, J. Electroanal. Chem., 10 (1965) 35; E. Dutkiewicz and R. Parsons, J. Electroanal. Chem., 11 (1966) 100.
24 M.J. Weaver and F.C. Anson, J. Electroanal. Chem., 65 (1975) 737.
25 J.W. Schultze and K.J. Vetter, J. Electroanal. Chem., 44 (1973) 63.
26 L. Pauling, The Nature of the Chemical Bond, 3rd ed., Cornell University Press, Ithaca, NY, 1960, p. 514.
27 J.T. Hupp, D. Larkin and M.J. Weaver, to be submitted for publication.
28 T. Vitanov, A. Popov and E.S. Sevast'yanov, Sov. Electrochem., 12 (1976) 557.
29 A.R. Sears and P.A. Lyons, J. Electroanal. Chem., 42 (1973) 69.
30 M.J. Weaver, F. Barz, J.G. Gordon and M.R. Philpott, Surf. Sci., submitted.
31 M.J. Weaver, J. Electroanal. Chem., 93 (1978) 231.

32 T.L. Satterberg and M.J. Weaver, J. Phys. Chem., 82 (1978) 1784.
33 R.Payne, Trans. Far. Soc., 64 (1968) 1638.
34 E.R. Gonzalez, J. Electroanal. Chem., 90 (1978) 431.
35 D.J. Barclay, J. Electroanal. Chem., 28 (1970) 443; D.J. Barclay and J. Čaja, Croat. Chem. Acta, 43 (1971) 221.
36 D.D. Bodé, Jr., J. Phys. Chem., 76 (1972) 2915.
37 J.W. Schultze and F.D. Koppitz, Electrochim. Acta, 21 (1976) 327.